Luminescence Quenching by Photoinduced Charge Transfer between Metal Complexes in Peptide Nucleic Acids

ARTICLE *in* THE JOURNAL OF PHYSICAL CHEMISTRY B · JUNE 2014

Impact Factor: 3.3 · DOI: 10.1021/jp5027042 · Source: PubMed

8 AUTHORS, INCLUDING:

Xing Yin

University of Pittsburgh

11 PUBLICATIONS **24** CITATIONS

SEE PROFILE

Yongle Li

New York University

21 PUBLICATIONS **248** CITATIONS

SEE PROFILE

Zhijie Ma

University of Colorado at Boulder

12 PUBLICATIONS **272** CITATIONS

SEE PROFILE

Catalina Achim

Carnegie Mellon University

60 PUBLICATIONS **1,745** CITATIONS

SEE PROFILE

THE JOURNAL OF PHYSICAL CHEMISTRY B

Article

Luminescence Quenching by Photoinduced Charge Transfer between Metal Complexes in Peptide Nucleic Acids

Xing Yin, Jing Kong, Arnie R. De Leon, Yongle Li, Zhijie Ma, Emil Wierzbinski, Catalina Achim, and David H. Waldeck

J. Phys. Chem. B, **Just Accepted Manuscript** • DOI: 10.1021/jp5027042 • Publication Date (Web): 27 Jun 2014

Luminescence Quenching by Photoinduced Charge Transfer between Metal Complexes in Peptide Nucleic Acids

Xing Yin,[a] Jing Kong,[b] Arnie De Leon,[b] Yongle Li,[c] Zhijie Ma,[b] Emil Wierzbinski,[a] Catalina Achim,[b]* and David H. Waldeck[a]*

[a] Department of Chemistry, University of Pittsburgh, Pittsburgh, PA 15260, United States

[b] Department of Chemistry, Carnegie Mellon University, Pittsburgh, PA 15213, United States

[c] Department of Chemistry, New York University, Manhattan, NY 10012, United States

*indicates corresponding author: achim@cmu.edu, dave@pitt.edu

Abstract

A new scaffold for studying photoinduced charge transfer has been constructed by connecting a $[Ru(Bpy)_3]^{2+}$ donor to a bis(8-hydroxyquinolinate)$_2$ copper [CuQ_2] acceptor through a peptide nucleic acid (PNA) bridge. The luminescence of the $[Ru(Bpy)_3]^{2+*}$ donor is quenched by electron transfer to the [CuQ_2] acceptor. Photoluminescence studies of these donor-bridge-acceptor systems reveal a dependence of the charge transfer on the length and sequence of the PNA bridge and on the position of the donor and acceptor in the PNA. In cases where the $[Ru(Bpy)_3]^{2+}$ can access the π base stack at the terminus of the duplex, the luminescence decay is described well by a single exponential; but if the donor is sterically hindered from accessing the π base stack of the PNA duplex, a distribution of luminescence lifetimes for the donor $[Ru(Bpy)_3]^{2+*}$ is observed. Molecular dynamics simulations are used to explore the donor-PNA-acceptor structure and the resulting conformational distribution provides a possible explanation for the distribution of electron transfer rates.

KEYWORDS: Electron transfer, lifetime distribution analysis, >time-resolved photoluminescence, conformational analysis, pi-stack

Introduction

Nucleic acids are interesting building blocks for supramolecular assemblies because of their predictable and programmable Watson-Crick base pairing, which in turn makes possible the encoding of specific three-dimensional architectures in the assemblies.[1-5] Hence nucleic acids have been studied extensively as a building block for nanotechnology applications.[6] Chemical synthesis has created either nucleic acid analogues, such as peptide nucleic acids (PNAs), or nucleic acids with functional groups, including redox centers and fluorophores, that impart functionality to the nucleic-acid-based nanostructures. This work reports on PNA, a synthetic analog of DNA that typically has a pseudo-peptide backbone composed of N-(2-aminoethyl)-glycine units.[7-9] PNA offers a number of advantages over DNA for nucleic acid based structures, such as higher thermal stability, superior chemical stability in biological media, and control over the chirality.[10,11] The PNA backbone and nucleobases have been chemically modified to confer desirable properties for specific applications, such as sequence specific binding to DNA, cell permeability, and others.[12,13] By substituting the PNA nucleobases with ligands that have a high affinity for metal ions, PNA duplexes that bind transition metal ions at specific positions can be created.[10,11]

While we and others have appended electroactive groups to PNA and reported the results of electrochemical and sensing studies of PNA attached to solid surfaces,[14-21] charge transfer through PNA duplexes in solution has not been reported. We have studied charge transfer through self-assembled monolayers (SAMs) of the PNAs by electrochemistry,[22,23] and more recently, we have measured the single molecule conductance of the PNAs by a break junction method and compared it to the electrochemical charge transfer rates.[24] Studies of unimolecular charge transfer in PNA, which possesses a neutral polyamide backbone rather than the diphosphate ester, polyanion backbone of DNA, provide insight into the fundamental features of long-range charge transfer in nucleic acids, by making possible comparisons with existing work on DNA[25-32,33-40] and eventually with other nucleic acids.

In this work, photoinduced electron transfer through PNA is studied between a $[Ru(Bpy)_3]^{2+}$ electron donor and a [Cu(8-hydroxy-quinolinate)$_2$] ([CuQ_2]), which acts as an electron acceptor. A PNA monomer that contains a $[Ru(Bpy)_3]^{2+}$ complex tethered to the PNA backbone was synthesized (Monomer **Ru** in Figure 1) and introduced into PNA oligomers at different positions,

either terminal or central, by solid phase peptide synthesis (Table 1 and S1). When $[Ru(Bpy)_3]^{2+}$ was situated in a central position of the duplex, an abasic PNA monomer in which the secondary amine of the Aeg was capped with an acetyl group (Monomer **B** in Fig 1) was introduced at the position complementary to $[Ru(Bpy)_3]^{2+}$. The acceptor was created by Cu^{2+} coordination to a pair of Q ligands situated in complementary positions in the duplexes (Monomer **Q** in Fig 1).[15]

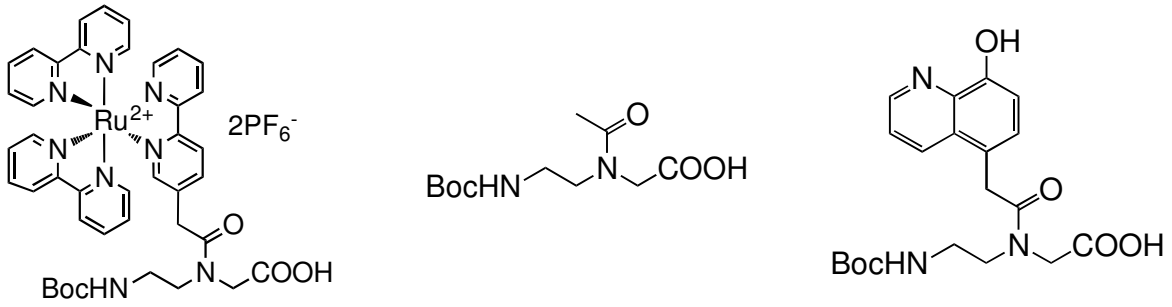

Ru **B** **Q**

Figure 1: The structure of PNA monomers. The nucleobase is replaced by $[Ru(Bpy)_3]^{2+}$ (Monomer **Ru**), formally, by a hydrogen atom (Monomer **B**), or by 8-hydroxyquinoline (Monomer **Q**).

Methods

PNA Synthesis and Characterization

Materials: The Boc-protected 8-hydroxyquinolinyl PNA monomer 2-(N-(tert-butyloxycarbonyl-2-aminoethyl)-2-(8-hydroxyquinolin-5-yl)acetamido)acetic acid (**Q**, Figure 1C) and precursor 2,2'-bipyridyl PNA monomer **1** (Figure 2) 2-(N-(tert-butyloxycarbonyl-2-aminoethyl)-2-(2,2'-bipyridin-4-yl)acetamido)acetic acid, which are needed for synthesizing ruthenium(II) tris(bipyridyl) PNA monomer (**Ru**, Figure 1A), were synthesized as reported previously.[15,41] The ruthenium(II) tris(bipyridyl) PNA monomer **Ru**, namely 2-(N-(tert-butyloxycarbonyl-2-aminoethyl)-2-(2,2'-bipyridin-4-yl) acetic acid)-bis(2,2'-bipyridine)ruthenium(II), was synthesized from precursor **1**, Bpy PNA monomer.[42] The backbone monomer was synthesized from the coupling between tert-butyl 2-(2-(tert-butoxycarbonyl)ethylamino)acetate and acetic anhydride, followed by hydrolysis, as reported previously.[22] All other reagents were commercially available, analytical grade quality, and used without further purification.

Synthesis of $[Ru(Bpy)_3]^{2+}$-containing PNA monomer (Figure 2): All manipulations were carried out under low light. Bpy PNA monomer **1** (415 mg, 1mmol) was suspended in 43 ml of a 70% ethanol solution. cis-Bis(2,2'-bipyridine)dichlororuthenium(II) hydrate (500 mg, 0.96 mmol) was added to the suspension. The reaction mixture was refluxed for 16 h and the solvent was removed by vacuum. The compound was purified by cation exchange chromatography using CM-sepharose resin, with an ammonium chloride step gradient. The desired product precipitated out of the solution upon addition of ammonium hexafluorophosphate. The precipitate was filtered and washed several times with water and ether. An orange residue remained. Yield: 42% (447 mg). Mass Spectral data (ESI) calc./found 827.9/827.2. ^{1}H NMR (300 MHz, CD_3CN): δ8.5 (m, 6H), 8.05 (m, 5H), 7.95 (m, 1H), 7.75 (m, 5H), 7.60 (m, 1H), 7.40 (m, 5H), 5.50 (βρ, 1H,NH), 4.0 (m, 2H, CH_2), 3.6 (m, 2H, CH_2), 3.30 (m, 2H, CH_2), 3.10 (m, 2H, CH_2), 1.40 (s, 9H, Boc).

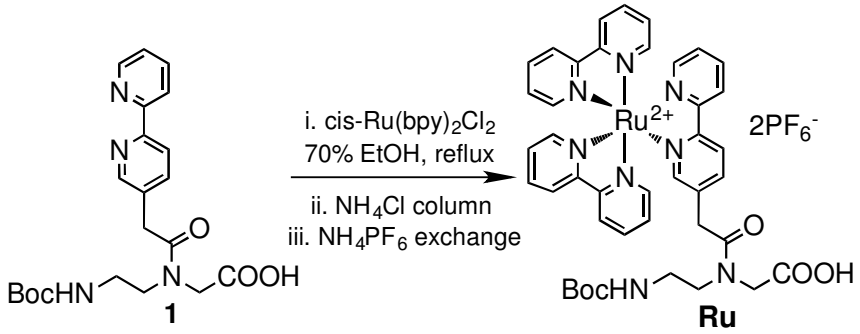

Figure 2*:* The synthesis scheme for the PNA monomer that contains $[Ru(Bpy)_3]^{2+}$ complex**.**

Solid Phase PNA Synthesis: PNA oligomers were synthesized with the Boc-protection strategy. PNA monomers were purchased from ASM Research Chemicals and were used without further purification. PNA was precipitated using diethyl ether after cleavage and was purified by reversed-phase HPLC using a C18 silica column on a Waters 600 model. Absorbance was measured at 260 nm with a Waters 2996 Photodiode Array Detector. The concentration of PNA oligomers was determined by UV absorption at 90°C using the sum of the extinction coefficients of the constituent PNA monomers at 260 nm taken from the literature. (ε_{260} were taken to be 8600 M^{-1} cm^{-1} for T, 6600 M^{-1} cm^{-1} for C, 13700 M^{-1} cm^{-1} for A, and 11700 M^{-1} cm^{-1} for G).[10] The extinction coefficient for the $[Ru(Bpy)_3]^{2+}$ at 260 nm is taken to be the same as that of

$[Ru(Bpy)_3]Cl_2$ in water (ε_{260} = 13250 $M^{-1}cm^{-1}$). The extinction coefficient for 8-hydroxyquinoline ε_{260} = 2570 M^{-1} cm^{-1} (at pH 7.0) was determined from the slope of a plot of A_{260} versus concentration.

Characterization of the oligomers was performed by MALDI-ToF mass spectrometry on an Applied Biosystems Voyager Biospectrometry Workstation with Delayed Extraction and an R-cyano-4-hydroxycinnamic acid matrix (10 mg/mL in 1:1 water/acetonitrile, 0.1% TFA). m/z for $(M+H)^+$ were calculated and found to be **P-AA** α 3565.44/3568.05, **P-AA** β 2879.88/2882.03, **P-AG** α 3582.63/3582.39, **P-AG** β 2864.87/2864.95, **P-AGTGA** α 3582.63/3579.06, **P-AGTGA** β 2864.87/2863.12, **P-AA-P'** α 4390.71/4392.44, **P-AA-P'** β 3824.73/3824.83, **P-AG-P'** α 4415.82/4417.45, **P-AG-P'** β 3799.10/3800.87.

Photoluminescence Measurement

Steady-state emission spectra were measured on a HORIBA Jobin Yvon Fluoromax 3 fluorescence spectrophotometer. The luminescence decay data were collected using the time-correlated single photon counting (TCSPC) method with a PicoHarp 300 TCSPC module (PicoQuant GmbH). The samples were excited by light from a 440 nm pulsed diode laser (PIL043, ALS GmbH) operating at a 500 kHz repetition rate. Emission from the sample was collected at 620 nm. All PNA samples were dissolved in 10 mM phosphate buffer (pH=7) and measurements were performed with a duplex concentration of 20 $\boldsymbol{\mu}$M. The concentration dependence was tested for **P-AA**/Cu, **P-AA-P'**/Cu, and **P-AG-P'**/Cu from 3 $\boldsymbol{\mu}$M to 30 $\boldsymbol{\mu}$M (see Table 1 for sequence of the PNAs). In each case, no concentration dependence of the luminescence lifetime was observed, indicating a unimolecular decay process. The instrument response function had a full-width-at-half-maximum (fwhm) of ~60ps, which is much shorter than the luminescence lifetimes (> 250 ns); thus tail fitting (discarding the rising part of the decay) was employed in the exponential component and lognormal distribution analyses.

Lognormal Distribution Fitting of Luminescence Decays

A general form of the luminescence decay law may be written as

$$D(t) = C_0 \cdot \int_0^{\infty} A(\tau)\ \exp\left(-\frac{t}{\tau}\right)\ \mathrm{d}\tau + B_0 \qquad \textbf{Equation 1}$$

where $D(t)$ is the emission intensity at time t and $A(\tau)$ is the normalized distribution function of luminescence lifetimes τ. C_0 is a parameter that represents the experimental signal at time zero, and B_0 represents the background counts (noise level). $D(t)$ is a Laplace transform of $A(\tau)$ and to recover $A(\tau)$ one can perform an inverse Laplace transform. Several methods exist for this purpose, such as the maximum entropy method[43] and a method for the recovery of $A(\tau)$ from frequency domain data.[44-46] These methods do not require *a priori* knowledge about the shape of the distribution but they are usually very sensitive to noise and require very high counts (about 5×10^5 counts per channel)[47] because of the ill-conditioned nature of inverse Laplace transforms.[48]

Here we assume a lognormal shape[47] of the lifetime components and perform a direct fitting of the data which is much more robust with regard to noise. The lognormal distribution is used because it has the correct boundary behaviors.[49] Using symbols similar to those used for the normal distribution, the lognormal distribution $P(\tau)$ is defined as:

$$P(\tau) = \frac{1}{\tau \cdot \sigma\sqrt{2\pi}} \exp\left\{\frac{-(\ln\tau - \mu)^2}{2\sigma^2}\right\} \qquad \textbf{Equation 2}$$

where μ is a parameter related to the peak maximum and σ is a parameter controlling the peak width. Note that μ and σ are not the mean and standard deviation of the distribution. Equation 2 can be transformed to

$$P(\tau) = \frac{1}{\sigma\sqrt{2\pi}} \cdot \exp\left(\frac{\sigma^2}{2} - \mu\right) \cdot \exp\left\{\frac{-[\ln\tau - (\mu - \sigma^2)]^2}{2\sigma^2}\right\} \qquad \textbf{Equation 3}$$

From the above equation, it is straightforward to show that the peak maximum (mode) is $\exp(\mu - \sigma^2)$ and the mean is $\exp(\mu + \sigma^2/2)$.

Another reason to choose the lognormal distribution is that a lognormal distribution of τ is equivalent to a lognormal distribution of the decay rate, k. Because $\tau = 1/k$, one finds that

$$P_\tau(\tau) = \exp\left\{\frac{-[\ln\tau - (\mu - \sigma^2)]^2}{2\sigma^2}\right\} = \exp\left\{\frac{-[\ln k - (\sigma^2 - \mu)]^2}{2\sigma^2}\right\} \qquad \textbf{Equation 4}$$

where $P_\tau(\tau) = \sigma\sqrt{2\pi}\, P(\tau) \cdot \exp\left(\frac{-\sigma^2}{2} + \mu\right)$. If one defines $\mu' = 2\sigma^2 - \mu$, then one obtains:

$$P_\tau(\tau) = \exp\left\{\frac{-[\ln k - (\mu' - \sigma^2)]^2}{2\sigma^2}\right\} = P_k(k) \qquad \textbf{Equation 5}$$

The overall distribution function $A(\tau)$ may contain more than one peak (two in the actual fitting used here) and it is defined as follows

$$A(\tau) = C_1 \cdot P_1(\tau) + C_2 \cdot P_2(\tau) + \cdots \quad \textbf{Equation 6}$$

where C_1 and C_2 are the normalized statistical weight of each peak. To fit $A(\tau)$ with experimental data, a set of discrete lifetimes (the number of lifetimes used is 200 in this work) from 1 ns to 1000 ns are used to convert the integral in Equation 1 to a summation; that is,

$$D(t) = C_0 \cdot \sum_k \left\{ A_k \cdot \exp\left(-\frac{t}{\tau_k}\right) \right\} + B_0 \quad \textbf{Equation 7}$$

where $A_n = A(\tau_n)$ is the amplitude of lifetime τ_n. The $D(t)$ defined above is used for the fit with experimental data. Because TCSPC data follows a Poisson distribution, the fitting process varies the A_n parameters in order to minimize the reduced chi-square χ^2:

$$\chi^2 = \sum_t \frac{[D(t) - F(t)]^2}{N \cdot F(t)} \quad \textbf{Equation 8}$$

where *N* is the number of TCSPC channels. χ^2 is set as the objective function and is optimized to a minimum by using the Optimization Toolbox in MATLAB. The final χ^2 is smaller than 1.05 for all lognormal distribution fittings.

Molecular Dynamic Simulation

The molecular dynamics (MD) simulation followed a protocol like that previously reported for PNAs.[50,51] The initial structures were constructed based on the average helicoidal parameters of experimentally determined PNA duplexes (PDB ID: 2K4G).[52] Because a force field is not available for the [CuQ_2] complex, an A:T base pair was used instead. The force field ff99SB[53] was complemented with the previously determined atomic partial charges[52] and the parameter set was adapted from another work[54] for $[Ru(Bpy)_3]^{2+}$. The structures were solvated in a TIP3P water box, such that the distance between the walls of the box and the closest PNA atom was at least 12 Å. After energy minimization and equilibration, the solvated structures were subjected to a 2 ns MD run using the module 'pmemd' of Amber 12[55] at T = 300 K and P = 1 atm, with periodic boundary conditions. A total of 10000 snapshots were saved for each trajectory (at every 1 ps) and used for the subsequent electronic structure calculations.

Results and Discussion

Duplex Characterization: The formation of the PNA duplexes and the binding of Cu^{2+} to the duplexes have been studied by thermal denaturation and by titrations using photoluminescence spectroscopy. Table 1 shows the sequence of several of the PNA duplexes that are studied in this work; see Table S1 for a more comprehensive list.[41,42] The sequence of the duplexes is related to that of the duplex named **P** in Table 1. The positions of the donor unit (labeled **Ru**) and of the ligands (labeled **Q**) that form the [CuQ_2] acceptor on the PNA duplexes are varied between the different systems studied. In addition, the chemical nature of the base pairs has been varied (see **P-AG** and **P-AA** in Table 1). For example, PNA duplexes that contain a terminal Ru donor and can form the [CuQ_2] acceptor have been synthesized with two or five nucleobases between the donor and acceptor positions. The name of these duplexes includes the names of the nucleobases situated between the donor and the acceptor; for example, duplex **P-AA** has two A nucleobases between the **Ru** monomer and **Q** ligand and can form two AT base pairs between the donor and the [CuQ_2] acceptor. Duplexes that have only one **Q** ligand (instead of a pair of **Q** ligands) have been synthesized as control systems and are labeled with a **1Q**. In addition, duplexes that have a duplex 'tail' which sterically hinders the $Ru(Bpy)_3^{2+}$ donor from accessing the duplex terminus were synthesized, and they are identified by including the tail in the name of the duplex as **P'**.

Table 1: Sequences and Melting Temperatures T_m of the PNA Duplexes with and without Cu^{2+}.[a]

Duplex	Sequence	T_m (°C)[b]	
		no Cu^{2+}	with Cu^{2+}
P	H–AGTGATCTAC–H H_2N–Lys–TCACTAGATG–H	67	67
P-AG	H–**Ru**AG**Q**GATCTAC–Lys–NH_2 H_2N–Lys–TC**Q**CTAGATG–H	56	>75
P-AA	H–**Ru**AA**Q**GATCTAC–Lys–NH_2 H_2N–Lys–TT**Q**CTAGATG–H	56	>75
P-AG-1Q	H–**Ru**AG**Q**GATCTAC–Lys–NH_2 H_2N–Lys–TCACTAGATG–H	58	52
P-AA-1Q	H–**Ru**AA**Q**GATCTAC–Lys–NH_2 H_2N–Lys–TTACTAGATG–H	58	56
P-AGTGA	H–**Ru**AGTGA**Q**CTAC–Lys–NH_2 H_2N–Lys–TCACT**Q**GATG–H	47	>75
P-AT-P'	H–AGTGA**Ru**AT**Q**TCTAC–Lys–NH_2 H_2N–Lys–TCACT**B**TA**Q**AGATG–H	48	70
P-AG-P'	H–AGTGA**Ru**AG**Q**TCTAC–Lys–NH_2	48	66

	H_2N-Lys-TCACT**B**TC**Q**AGATG-H

[a] Ru, Q, and B indicate the monomers in Fig 1; T, C, G, and A are the conventional nucleobase notations; and Lys indicates placement of a lysine; [b] The T_m values are an average of 2 or 3 measurements on 5 μM solutions of ds PNA in a pH 7.0, 10 mM sodium phosphate buffer solution and are known within 1°C.

Melting curves of PNA duplexes in the absence and presence of Cu^{2+} are shown in panels A and B of Figure 3; the melting temperatures T_m for all the duplexes are reported in Table 1. The T_m of the non-modified, 10-base pair PNA duplex **P** is 67°C. The T_m of duplexes that contained one or two Q ligands was lower than that of **P** by 9-20°C. This decrease is similar to that caused by a base pair mismatch. In the presence of Cu^{2+}, the melting of the **P-AG**, **P-AA**, and **P-AGTGA** duplexes showed a hyperchromicity increase of more than 15% as the temperature was

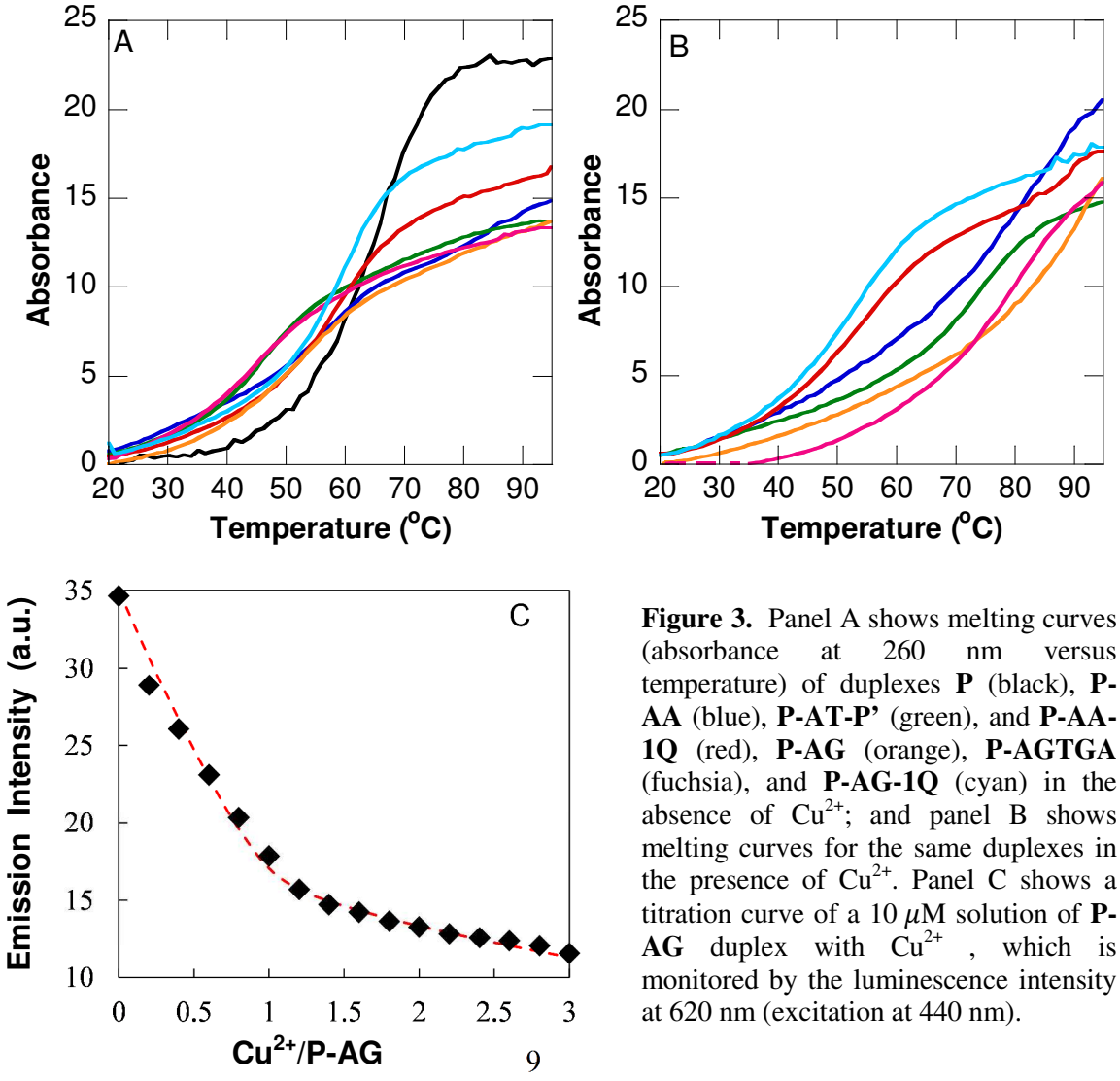

Figure 3. Panel A shows melting curves (absorbance at 260 nm versus temperature) of duplexes **P** (black), **P-AA** (blue), **P-AT-P'** (green), and **P-AA-1Q** (red), **P-AG** (orange), **P-AGTGA** (fuchsia), and **P-AG-1Q** (cyan) in the absence of Cu^{2+}; and panel B shows melting curves for the same duplexes in the presence of Cu^{2+}. Panel C shows a titration curve of a 10 μM solution of **P-AG** duplex with Cu^{2+}, which is monitored by the luminescence intensity at 620 nm (excitation at 440 nm).

increased, but the hyperchromicity did not reach saturation. In these cases a two-state model cannot be used to determine the T_m but the increase in hyperchromicity indicates that the duplexes are stabilized by Cu^{2+}. For the other PNA duplexes, the melting curves measured in the presence of Cu^{2+} reached saturation, and the T_m determined using a two-state model was higher than that of duplex **P** by more than 15°C.[56] This increase in stability in the presence of Cu^{2+} for all PNA duplexes that contain a pair of **Q** ligands could be attributed to the formation of a $[CuQ_2]$ complex that functions as an alternative base pair. This interpretation of the melting temperature data is supported by the fact that the T_m of the PNA duplexes that contain only one **Q** ligand and cannot form an intra-duplex $[CuQ_2]$ complex (**P-AG-1Q** and **P-AA-1Q**) was 9°C lower than that of **P** and was not stabilized by Cu^{2+}.

Photoluminescence titrations of the duplexes (Figure 3C and Figure S1) showed a decrease in the emission intensity of $[Ru(Bpy)_3]^{2+}$ as the Cu^{2+} concentration increased. This decrease can be described by a bimolecular equilibrium between the Cu^{2+}-free duplex and the duplex to which one equivalent of Cu^{2+} is coordinated (in which the luminescence of the Ru complex is quenched; see Supporting Information).[43,45-49,57-60] The equilibrium constant from this analysis was found to be larger than $10^6\ M^{-1}$.[61] The photoluminescence measurements described below were performed on 10 μM to 20 μM solutions of the PNA duplexes that contained two equivalents of Cu^{2+}; under these conditions a K~ $10^6\ M^{-1}$ implies that 97% of the duplexes are fully coordinated with Cu^{2+}.

Charge Transfer and the Duplex π-stack: The luminescence decay profiles for **P-AG** and **P-AGTGA** duplexes, which are presented in Figure 4, show the effect of the [CuQ_2] acceptor on the $[Ru(Bpy)_3]^{2+*}$ luminescence. In the absence of Cu^{2+}, the luminescence intensity of the $[Ru(Bpy)_3]^{2+*}$ complex in the **P-AG** and **P-AGCTA** duplexes (Figure S3) is similar to that of the "free" $[Ru(Bpy)_3]^{2+*}$ complex in solution (Figure S2). Addition of Cu^{2+} to the solution of the duplexes modified with **Ru**, but with no **Q** ligands, left the luminescence of $[Ru(Bpy)_3]^{2+*}$ unaffected (Figure S5). In contrast, the addition of one or more equivalents of Cu^{2+} to a solution of duplexes that contain two **Q** ligands quenches the $[Ru(Bpy)_3]^{2+*}$ luminescence (Fig 3). These results indicate that quenching of the $[Ru(Bpy)_3]^{2+*}$ in the **P-AG** or **P-AGCTA** involves the [CuQ_2] complex that is part of the PNA duplex. Energy transfer from $[Ru(Bpy)_3]^{2+*}$ to [CuQ_2] is discounted as a decay pathway because of the poor overlap between the emission spectrum of $[Ru(Bpy)_3]^{2+}$ (Figure S2 and Figure S4) and the absorption spectrum of [CuQ_2] (Figure S3). On the other hand, the electron transfer reaction $[Ru(Bpy)_3]^{2+*}$+[CuQ_2] → $[CuQ_2]^-$ + $[Ru(Bpy)_3]^{3+}$ is thermodynamically favorable (ΔG < -0.6 eV before Coulomb correction,[62,63] see SI). Hence, quenching of the $[Ru(Bpy)_3]^{2+*}$ occurs because of electron transfer to the acceptor [CuQ_2]. This conclusion was corroborated by the observation of strong luminescence with the redox inactive [ZnQ_2] in the **P-AG** duplex (see SI for details). Note that a conformational change between [CuQ_2] and $[CuQ_2]^-$ may occur after charge transfer; however, the reduction potential of $[Ru(Bpy)_3]^{3+}$ is much more positive (+1.15 V vs. NHE) (See Supporting Information) than that of [CuQ_2] (+0.05 V vs. NHE)[62] and a fast back electron transfer in the ground state is expected

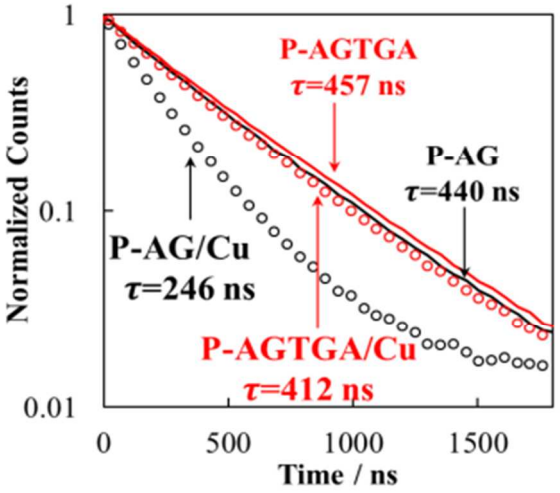

Figure 4: Luminescence decay for 20 μM solutions of **P-AG** (black) and **P-AGTGA** (red) in a pH 7.0, 10 mM phosphate buffer in the absence (solid lines) and presence (open circles) of two Cu^{2+} equiv. The time constants that are obtained from a best fit by a single exponential decay are shown in the figure. A support plane analysis (see supplemental information) indicates that they are accurate to ± 1 ns; however sample to sample variations display a standard deviation of ~ 1.5% in the lifetime value (see section 5 of the Supplementary Information).

to restore the planar structure of the [CuQ_2] complex. This interpretation is supported by the fact that the system showed no signs of photoinduced degradation over the course of the experiments.

The luminescence decays for $[Ru(Bpy)_3]^{2+*}$ in duplexes of **P-AG** and **P-AGTGA** were used to probe the length dependence of the charge transfer rate; see Fig 4. In each case the luminescence decay law could be described by a single exponential,[64] and the addition of Cu^{2+} caused a decrease of the luminescence lifetime of the $[Ru(Bpy)_3]^{2+*}$ for both duplexes. Assuming that the enhanced excited state decay rate of $[Ru(Bpy)_3]^{2+*}$ upon addition of Cu^{2+} is caused by electron transfer, the rate constant for electron transfer from $[Ru(Bpy)_3]^{2+*}$ to [CuQ_2] can be calculated as $k_{CT} = 1/\tau - 1/\tau_0$; one obtains a value of 1.8 μs^{-1} for **P-AG** and of 0.24 μs^{-1} for **P-AGTCA**. Although these values are for only two donor-acceptor distances, a decay parameter of $\beta \sim 0.2$ $Å^{-1}$ is obtained if one assumes that $k_{CT} \propto \exp(-\beta \cdot D_{DA})$, in which D_{DA} is the distance between $[Ru(Bpy)_3]^{2+*}$ and [CuQ_2] through the π-base stack. This value should be considered a lower limit however; as differences in $\Delta_r G$ for the **P-AG** than **P-AGTGA** duplexes that arise from differences in the Coulomb field stabilization of the different charge separated states also affect the rate constant.[68,69] Accounting for these differences causes the value of β to increase to about 0.4 $Å^{-1}$ (see section 5 of SI). Nevertheless, the value of β lies between the values reported for superexchange in single stranded PNAs (0.7~0.8 $Å^{-1}$)[23,62,65] and hole hopping in duplex PNAs (0.07 $Å^{-1}$)[65] from electrochemistry. The difference between β measured by luminescence in solution and by electrochemistry in SAMs of PNA may be caused by differences in the PNA geometry and/or by the fact that the charge transfer is likely to be electron-mediated[66,67] in solution and hole-mediated[23,65] in the SAMs.

The distance dependence observed here for PNA is consistent with literature reports for DNA. The range of estimated β values (0.2 to 0.4) for PNA are somewhat smaller than those reported for DNA in the superexchange regime, which range from 0.6-0.8,[31,70-72] but are comparable to the range of β values (0.2-0.4) $Å^{-1}$ reported for hole transfers in DNA when the donor and acceptor are separated by 3-6 base pairs.[73,74] Note that β in DNA becomes < 0.1 $Å^{-1}$ once the hole transfer is in the hopping regime.[71] For reductive electron transfer in DNA, fewer studies are available and the mechanism is not yet wholly clear, but a number of groups have reported small β values for relatively short distances (less than 5 to 7 base pairs), ranging from 0.11 $Å^{-1}$ to 0.26 $Å^{-1}$.[66,67,75-77] Thus, the distance dependence observed here for photoinduced electron transfer

in PNA is not atypical of that found for charge transfer through π-stacked nucleobases in previous studies.

To examine the importance of the π-stack between the Ru donor and acceptor on the electron transfer, the effects (1) of a base pair mismatch and (2) of the chemical nature of the base pairs situated between the donor and acceptor were studied. To create a mismatch, a T nucleobase was replaced by a C nucleobase in one of the two AT base pairs situated between the $[Ru(Bpy)_3]^{2+}$ and the Q ligands in the **P-AA** duplex. The lifetime of Ru increased from 278 ns for the fully matched **P-AA**/Cu^{2+} duplex to 300 ns for the mismatched duplex in the presence of Cu^{2+}. This slowing of the charge transfer (longer lifetime) occurs, even though the mismatch is expected to cause more 'fraying' on the end of the base stack and suggests that the $Ru(Bpy)_3^{2+}$ is not penetrating through to the $[CuQ_2]$. For the fully complementary duplexes **P-AA** and **P-AG**, the difference in luminescence lifetime (278 ns for **P-AA/** Cu^{2+} and 265 ns for **P-AG/** Cu^{2+}) is smaller than that found in the mismatch study. This weak dependence on sequence is consistent with previous work on DNA for excess-electron transfer and has been attributed to the very similar reduction potentials of the base pairs.[66,67,78] These findings are consistent with charge transfer through the π-stack that is 'electron mediated'. Given the small lifetime changes, this hypothesis was tested further by constructing PNA duplexes in which the Ru is centrally situated and thus its access to the base stack is sterically encumbered.

Electron Transfer in Sterically Hindered Duplexes: The luminescence decay of the $[Ru(Bpy)_3]^{2+*}$ complex depends on the position of the Ru complex in the duplex, *i.e.* terminal versus central, as can be seen by comparing the data for **P-AG** and **P-AG-P'** in the presence of Cu^{2+} (Figure 5A). The **P-AG** duplex has the $[Ru(Bpy)_3]^{2+}$ at the end of the base stack while the **P-AG-P'** duplex is elongated so that the $[Ru(Bpy)_3]^{2+}$ cannot access the top of the nucleobase stack. The excited state decay law of $[Ru(Bpy)_3]^{2+*}$ in the **P-AG-P'** duplex cannot be fit by a single exponential; it could be fit by a double exponential decay law, however.

To quantify the difference between the **P-AG**/Cu and **P-AG-P'**/Cu decay laws, the χ^2 surface of a double exponential fit of the two decays was analyzed. In this analysis the ratio of the two lifetime components (τ_2/τ_1) was kept fixed while their absolute values and the relative amplitudes of the two decay components were varied to minimize the χ^2. Figure 5B shows a plot

of the optimized χ^2 for the two decay laws as a function of $\ln(\tau_2/\tau_1)$, where τ_1 and τ_2 are the two decay constants of the double exponential decay law. Note that when $\tau_2 = \tau_1$ (or $\ln(\tau_2/\tau_1) = 0$) a single exponential is recovered. It is clear from the plots that the **P-AG**/Cu system is better described by a single exponential (i.e., lower χ^2 value at $\ln(\tau_2/\tau_1) = 0$) than is the **P-AG-P'**/Cu system, and the χ^2 value of 1.4 for $\ln(\tau_2/\tau_1) = 0$ for **P-AG**/Cu is low enough to be considered acceptable for a single exponential fit. Moreover, the χ^2 versus $\ln(\tau_2/\tau_1)$ curve reaches a minimum at $\ln(\tau_2/\tau_1)$ =0.94 for **P-AG**/Cu whereas it is 1.31 for the centrally-attached **P-AG-P'**/Cu; again suggesting that **P-AG**/Cu is closer to a single exponential decay.

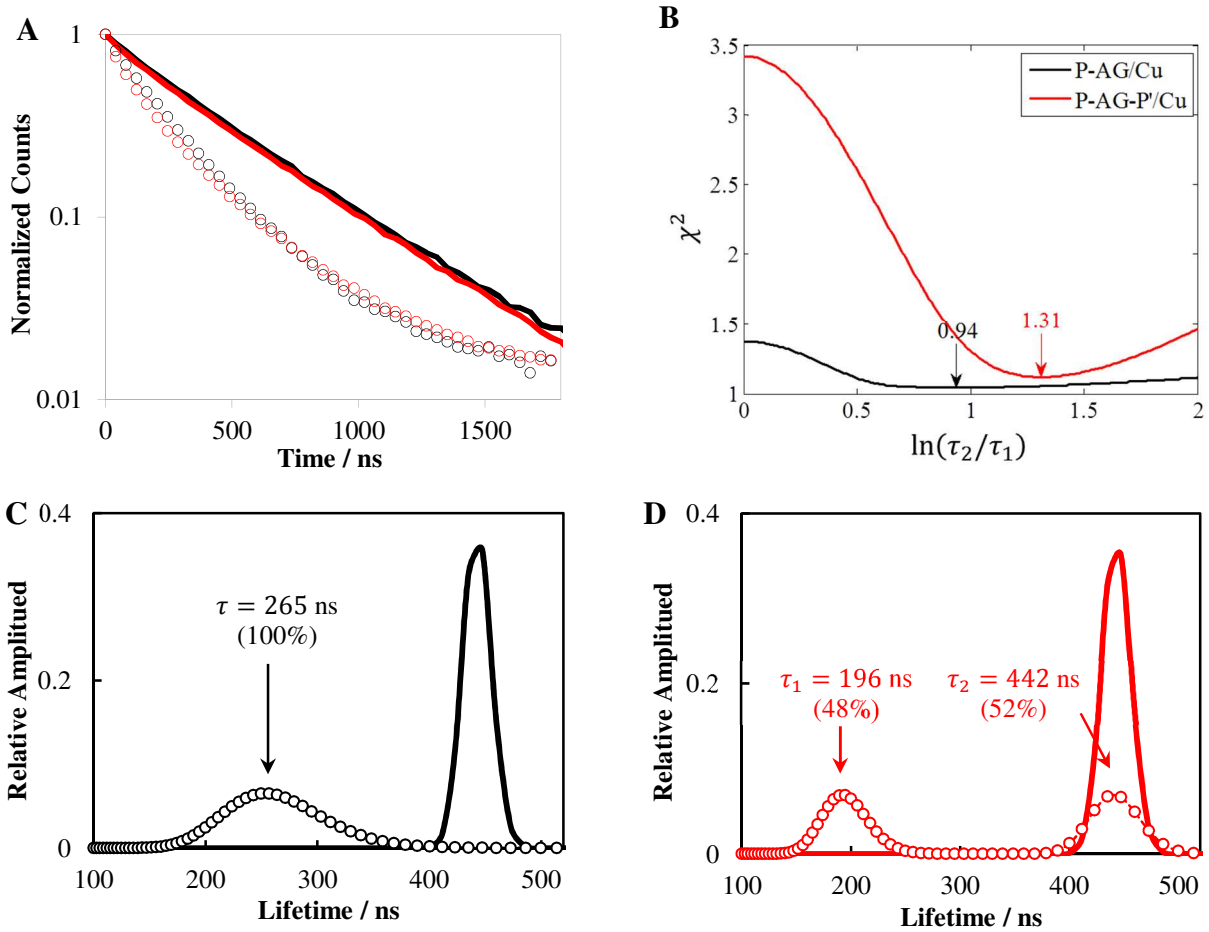

Figure 5: (A) Luminescence decays are shown for $[Ru(Bpy)_3]^{2+*}$ emission in duplexes **P-AG** (black) and **P-AG-P'** (red) in the absence (solid lines) and presence (open circles) of Cu^{2+}. Note that only every tenth data point is shown, so as to improve clarity of the image. (B) The optimized χ^2 of a double exponential

fit is plotted versus $\ln(\tau_2/\tau_1)$ for **P-AG** (black) and **P-AG-P'** (red) in the presence of Cu^{2+}. (C,D) The distribution of lifetimes are shown for the $[Ru(Bpy)_3]^{2+*}$ luminescence decay law. The color and symbol code is the same as panel A. Note that the distributions for the two duplexes in the absence of Cu^{2+} coincide and are centered at **442** ns. The mean value and the relative statistical weight of each peak are labeled for **P-AG/**Cu and **P-AG-P'/**Cu in panels C and D.

The origin of the difference in χ^2 values (Figure 5B) is revealed by the lognormal lifetime distribution analysis (procedure described in the Methods section) as shown in Figs 5C and 5D. Note that without Cu^{2+} present the distribution of $[Ru(Bpy)_3]^{2+*}$ luminescence lifetimes in **P-AG** and **P-AG-P'** are well described by a single exponential decay law, and the distribution plots in Fig 5C and 5D provide a lower limit on the peak width that is available from this analysis. In the presence of Cu^{2+}, the luminescence decay of the $[Ru(Bpy)_3]^{2+*}$ in **P-AG-P'** requires a bimodal distribution, whereas **P-AG** can be fit by a single mode distribution (albeit with a somewhat larger peak width than shown for the Cu^{2+} free case). The mean value for the long lifetime component of **P-AG-P'** in the presence of Cu^{2+} is similar to the mean lifetime observed for **P-AG** and **P-AG-P'** in the absence of Cu^{2+}, but it has a larger width.

The observation of two different lifetimes for **P-AG-P'** and a single lifetime for **P-AG** could be caused by differences in the conformations available for the $[Ru(Bpy)_3]^{2+}$ in these duplexes. The bimodal distribution of luminescence lifetimes observed for **P-AG-P'** suggests that the PNA exists in (at least) two distinct conformations for which the charge transfer rates between the $[Ru(Bpy)_3]^{2+*}$ and the $[CuQ_2]$ are significantly different and that the interchange between the two conformations is slow compared to the timescale of charge transfer. In contrast, the single mode distribution for the luminescence decay of the $[Ru(Bpy)_3]^{2+*}$ complex **in P-AG** in the presence of Cu^{2+} indicates that the $[Ru(Bpy)_3]^{2+*}$ complex adopts one dominant conformation with respect to the $[CuQ_2]$ acceptor (or several ones that interconvert fast on the charge transfer timescale).

This interpretation was corroborated by performing studies which showed that the luminescence decay of **P-AG -P'/**Cu^{2+}did not change when a mismatch was introduced between the $[Ru(Bpy)_3]^{2+*}$ and the $[CuQ_2]$.

In order to further test the conformation hypothesis, molecular dynamics (MD) simulations of the **P-AG** and **P-AG-P'** were performed. In these calculations, the $[CuQ_2]$ complex was replaced by an AT base pair because an accurate $[CuQ_2]$ force field is not yet available. Figure 6 shows the average structures of the duplexes that arise from typical trajectories and the

distributions that were found for the donor-to-acceptor distance. Figure 6A shows the case of **P-AG** for which one of the three bipyridine ligands participates in a π-π interaction with a terminal base pair. This interaction may restrict the flexibility of the $[Ru(Bpy)_3]^{2+}$ and favor positions of the complex in which π- π stacking between pyridine ligands and the A-T base pair occurs. Note that the steric interactions between the two $[Ru(Bpy)_3]^{2+}$ enantiomers and the left-handed PNA duplex are somewhat different (See SI for distributions of individual trajectories for PNAs that contain (Λ)- and (Δ)-$[Ru(Bpy)_3]^{2+}$) and may contribute to broadening of the distribution; see Figure 6C. For the **P-AG-P'** duplex the π-π interaction is less important; presumably because of the large steric effect that prevents $[Ru(Bpy)_3]^{2+}$ from intercalating into the π-stack. In this latter system, the central $[Ru(Bpy)_3]^{2+}$ can be flipped toward either end of the duplexes, resulting in a more complicated conformational distribution.

To quantitatively characterize the distributions, the donor-acceptor distance D_{DA} was calculated for snapshots of each trajectory at every 0.2 ps. D_{DA} is defined as the distance between the Ru atom and the centroid of the "acceptor" AT base pair. As shown in the histogram of Fig 6A, the D_{DA} for the duplexes with a terminal $[Ru(Bpy)_3]^{2+}$ complex have a single mode distribution; while for the duplexes with a central $[Ru(Bpy)_3]^{2+}$ complex the distribution is bimodal (see Fig 6B). Moreover, the mean value of the short-distance peak in duplexes with a terminal $[Ru(Bpy)_3]^{2+}$ complex is smaller than the corresponding value for duplexes with a central $[Ru(Bpy)_3]^{2+}$ complex, indicating that the latter duplexes would have a shorter

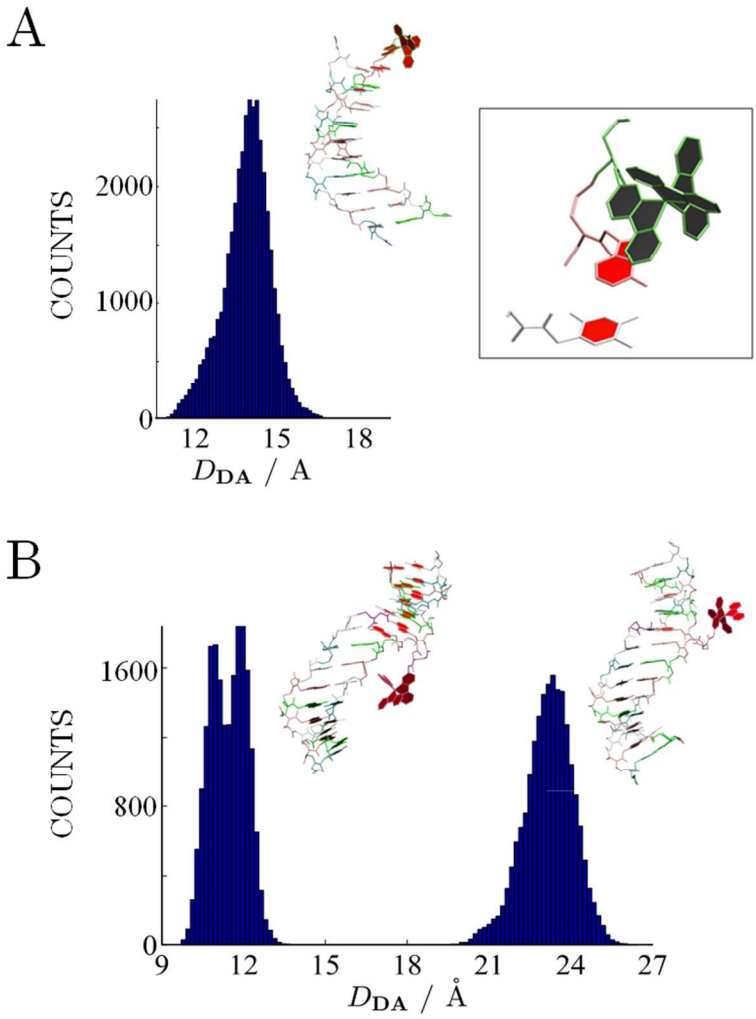

Figure 6. The D_{DA} distributions calculated using MD simulations for the analog of P-AG (A) and of P-AG-P' (B). The insets are the average structure for one MD trajectory. The aromatic rings of the Bpy in $[Ru(Bpy)_3]^{2+}$ are shown in green.

luminescence lifetime than the former ones, as observed in experiments. An alternative definition of D_{DA} was also considered but it gives rise to the same conclusions; see the Supporting Information for details.

Conclusions

In summary, this work demonstrates that $[Ru(Bpy)_3]^{2+*}$ can transfer an electron to a $[CuQ_2]$ complex incorporated into the nucleobase stack of a PNA duplex. If the $[Ru(Bpy)_3]^{2+}$ complex can access the terminus of the duplex and interact with the nucleobase π system, the electron transfer occurs through the nucleobase stack and is affected by mismatches and the number of nucleobase pairs between the donor and acceptor. If the $[Ru(Bpy)_3]^{2+}$ cannot access the PNA terminus, charge transfer can still proceed directly from the $[Ru(Bpy)_3]^{2+*}$ to the $[CuQ_2]$ if they are close enough, however the charge transfer rate does not depend on the mismatches or the intervening nucleobase pairs.

Supporting Information

The completed table of PNA sequences, titration curves of **P-AG-P'** and **P-AA**, Zn(II) control results, χ^2 analysis of the luminescence decay, the estimation of k_{CT}^0, more details of the molecular dynamics simulations. This material is available free of charge via the Internet at http://pubs.acs.org.

Acknowledgements

The authors acknowledge support from the U.S. National Science Foundation through grants CHE 1057981 to DHW and 1059037 to CA. We thank Dr. Marcela Madrid (PSC) for useful discussions on the MD simulations. Computational resources were provided by the Center for Simulation and Modeling (SaM) at the University of Pittsburgh.

References

(1) Rothemund, P. W. K. Folding DNA to Create Nanoscale Shapes and Patterns. *Nature* **2006**, *440*, 297-302.

(2) Dietz, H.; Douglas, S. M.; Shih, W. M. Folding DNA into Twisted and Curved Nanoscale Shapes. *Science* **2009**, *325*, 725-730.

(3) Yan, H. Materials Science. Nucleic Acid Nanotechnology. *Science* **2004**, *306*, 2048-2049.

(4) Bhatia, D.; Sharma, S.; Krishnan, Y. Synthetic, Biofunctional Nucleic Acid-Based Molecular Devices. *Curr. Opin. Biotechnol.* **2011**, *22*, 475-484.

(5) Krishnan, Y.; Simmel, F. C. Nucleic Acid Based Molecular Devices. *Angew. Chem., Int. Ed.* **2011**, *50*, 3124-3156.

(6) Seeman, N. C. Nanomaterials Based on DNA. *Annu. Rev. Biochem.* **2010**, *79*, 65-87.

(7) Koshkin, A. A.; Singh, S. K.; Nielsen, P.; Rajwanshi, V. K.; Kumar, R.; Meldgaard, M.; Olsen, C. E.; Wengel, J. Lna (Locked Nucleic Acids): Synthesis of the Adenine, Cytosine, Guanine, 5-Methylcytosine, Thymine and Uracil Bicyclonucleoside Monomers, Oligomerisation, and Unprecedented Nucleic Acid Recognition. *Tetrahedron* **1998**, *54*, 3607-3630.

(8) Egholm, M.; Nielsen, P. E.; Buchardt, O.; Berg, R. H. Recognition of Guanine and Adenine in DNA by Cytosine and Thymine Containing Peptide Nucleic Acids (Pna). *J. Am. Chem. Soc.* **1992**, *114*, 9677-9678.

(9) Schoning, K.-U. Chemical Etiology of Nucleic Acid Structure: The Alpha - Threofuranosyl-(3'rightarrow 2') Oligonucleotide System. *Science* **2000**, *290*, 1347-1351.

(10) Nielsen, P. E. *Peptide Nucleic Acids: Protocols and Applications*; 2 ed.; Taylor & Francis, 2004.

(11) Achim, C.; A. Armitage, B.; H. Ly, D.; W. Schneider, J.; Begley, T. P. In *Wiley Encyclopedia of Chemical Biology*; John Wiley & Sons, Inc.: 2007.

(12) Rozners, E. Recent Advances in Chemical Modification of Peptide Nucleic Acids. *J. Nucleic Acids* **2012**, *2012*, 518162.

(13) Nielsen, P. E. Peptide Nucleic Acids (Pna) in Chemical Biology and Drug Discovery. *Chem. Biodiversity* **2010**, *7*, 786-804.

(14) De Leon, A.; Kong, J.; Achim, C. In *Metallofoldamers: Supramolecular Architectures from Helicates to Biomimetics*; 1 ed.; Maayan, G., Albrecht, M., Eds.; John Wiley & Sons, Ltd: 2013, p 333-378.

(15) Watson, R. M.; Skorik, Y. A.; Patra, G. K.; Achim, C. Influence of Metal Coordination on the Mismatch Tolerance of Ligand-Modified Pna Duplexes. *J. Am. Chem. Soc.* **2005**, *127*, 14628-14639.

(16) Ma, Z.; Olechnowicz, F.; Skorik, Y. A.; Achim, C. Metal Binding to Ligand-Containing Peptide Nucleic Acids. *Inorg. Chem.* **2011**, *50*, 6083-6092.

(17) Nickita, N.; Gasser, G.; Bond, A. M.; Spiccia, L. Synthesis, Spectroscopic Properties and Electrochemical Oxidation of Ruii-Polypyridyl Complexes Attached to a Peptide Nucleic Acid Monomer Backbone. *Eur. J. Inorg. Chem.* **2009**, *2009*, 2179-2186.

(18) Joshi, T.; Barbante, G. J.; Francis, P. S.; Hogan, C. F.; Bond, A. M.; Gasser, G.; Spiccia, L. Electrochemiluminescent Monomers for Solid Support Syntheses of Ru(Ii)-Pna Bioconjugates: Multimodal Biosensing Tools with Enhanced Duplex Stability. *Inorg. Chem.* **2012**, *51*, 3302-3315.

(19) Metzler-Nolte, N. In *Bioorganometallics*; Wiley-VCH Verlag GmbH & Co. KGaA: 2006, p 125-179.

(20) Huesken, N.; Gebala, M.; Battistel, A.; La Mantia, F.; Schuhmann, W.; Metzler-Nolte, N. Impact of Single Basepair Mismatches on Electron-Transfer Processes at Fc-Pna Center Dot DNA Modified Gold Surfaces. *ChemPhysChem* **2012**, *13*, 131-139.

(21) Baldoli, C.; Rigamonti, C.; Maiorana, S.; Licandro, E.; Falciola, L.; Mussini, P. R. A New Triferrocenyl-Tris(Hydroxymethyl)Aminomethane Derivative as a Highly Sensitive

Electrochemical Marker of Biomolecules: Application to the Labelling of Pna Monomers and Their Electrochemical Characterization. *Chem.--Eur. J.* **2006**, *12*, 4091-4100.

(22) Wierzbinski, E.; de Leon, A.; Davis, K. L.; Bezer, S.; Wolak, M. A.; Kofke, M. J.; Schlaf, R.; Achim, C.; Waldeck, D. H. Charge Transfer through Modified Peptide Nucleic Acids. *Langmuir* **2012**, *28*, 1971-1981.

(23) Paul, A.; Watson, R. M.; Lund, P.; Xing, Y.; Burke, K.; He, Y.; Borguet, E.; Achim, C.; Waldeck, D. H. Charge Transfer through Single-Stranded Peptide Nucleic Acid Composed of Thymine Nucleotides. *J. Phys. Chem. C* **2008**, *112*, 7233-7240.

(24) Wierzbinski, E.; Venkatramani, R.; Davis, K. L.; Bezer, S.; Kong, J.; Xing, Y.; Borguet, E.; Achim, C.; Beratan, D. N.; Waldeck, D. H. The Single-Molecule Conductance and Electrochemical Electron-Transfer Rate Are Related by a Power Law. *ACS Nano* **2013**, *7*, 5391-5401.

(25) Schuster, G. B. Long-Range Charge Transfer in DNA: Transient Structural Distortions Control the Distance Dependence. *Acc. Chem. Res.* **2000**, *33*, 253-260.

(26) Kanvah, S.; Joseph, J.; Schuster, G. B.; Barnett, R. N.; Cleveland, C. L.; Landman, U. Oxidation of DNA: Damage to Nucleobases. *Acc. Chem. Res.* **2009**, *43*, 280-287.

(27) Shao, F.; O'Neill, M. a.; Barton, J. K. Long-Range Oxidative Damage to Cytosines in Duplex DNA. *Proc. Natl. Acad. Sci. U. S. A.* **2004**, *101*, 17914-17919.

(28) Stemp, E. D. a.; Arkin, M. R.; Barton, J. K. Oxidation of Guanine in DNA by Ru(Phen) 2 (Dppz) 3+ Using the Flash-Quench Technique. *J. Am. Chem. Soc.* **1997**, *119*, 2921-2925.

(29) Wagenknecht, H.-A. Reductive Electron Transfer and Transport of Excess Electrons in DNA. *Angew. Chem., Int. Ed.* **2003**, *42*, 2454-2460.

(30) Giese, B.; Amaudrut, J.; Köhler, A. K.; Spormann, M.; Wessely, S. Direct Observation of Hole Transfer through DNA by Hopping between Adenine Bases and by Tunnelling. *Nature* **2001**, *412*, 318-320.

(31) Meggers, E.; Michel-Beyerle, M. E.; Giese, B. Sequence Dependent Long Range Hole Transport in DNA. *J. Am. Chem. Soc.* **1998**, *120*, 12950-12955.

(32) Senthilkumar, K.; Grozema, F. C.; Guerra, C. F.; Bickelhaupt, F. M.; Lewis, F. D.; Berlin, Y. A.; Ratner, M. A.; Siebbeles, L. D. A. Absolute Rates of Hole Transfer in DNA. *J. Am. Chem. Soc.* **2005**, *127*, 14894-14903.

(33) Fukui, K.; Tanaka, K. Distance Dependence of Photoinduced Electron Transfer in DNA. *Angew. Chem., Int. Ed.* **1998**, *37*, 158-161.

(34) Genereux, J. C.; Barton, J. K. Mechanisms for DNA Charge Transport. *Chem. Rev.* **2010**, *110*, 1642-1662.

(35) Holmlin, R. E.; Stemp, E. D. a.; Barton, J. K. Os(Phen) 2 Dppz 2+ in Photoinduced DNA-Mediated Electron Transfer Reactions. *J. Am. Chem. Soc.* **1996**, *118*, 5236-5244.

(36) Murphy, C.; Arkin, M.; Jenkins, Y.; Ghatlia, N.; Bossmann, S.; Turro, N.; Barton, J. Long-Range Photoinduced Electron Transfer through a DNA Helix. *Science* **1993**, *262*, 1025-1029.

(37) Kumar, C. V.; Barton, J. K.; Turro, N. J. Photophysics of Ruthenium Complexes Bound to Double Helical DNA. *J. Am. Chem. Soc.* **1985**, *107*, 5518-5523.

(38) Brun, A.; Harriman, A. Dynamics of Electron Transfer between Intercalated Polycyclic Molecules: Effect of Interspersed Bases. *J. Am. Chem. Soc.* **1992**, *114*, 3656-3660.

(39) Lewis, F. D.; Letsinger, R. L.; Wasielewski, M. R. Dynamics of Photoinduced Charge Transfer and Hole Transport in Synthetic DNA Hairpins. *Acc. Chem. Res.* **2001**, *34*, 159-170.

(40) Lewis, F. D.; Wu, T.; Zhang, Y.; Letsinger, R. L.; Greenfield, S. R.; Wasielewski, M. R. Distance-Dependent Electron Transfer in DNA Hairpins. *Science* **1997**, *277*, 673-676.

(41) Franzini, R. M.; Watson, R. M.; Patra, G. K.; Breece, R. M.; Tierney, D. L.; Hendrich, M. P.; Achim, C. Metal Binding to Bipyridine-Modified Pna. *Inorg. Chem.* **2006**, *45*, 9798-9811.

(42) Kise, K. J.; Bowler, B. E. A Ruthenium(Ii) Tris(Bipyridyl) Amino Acid: Synthesis and Direct Incorporation into an Alpha-Helical Peptide by Solid-Phase Synthesis. *Inorg. Chem.* **2002**, *41*, 379-386.

(43) Livesey, a. K.; Brochon, J. C. Analyzing the Distribution of Decay Constants in Pulse-Fluorimetry Using the Maximum Entropy Method. *Biophys. J.* **1987**, *52*, 693-706.

(44) Alcala, J. R.; Gratton, E.; Prendergast, F. G. Interpretation of Fluorescence Decays in Proteins Using Continuous Lifetime Distributions. *Biophys. J.* **1987**, *51*, 925-936.

(45) Alcala, J. R.; Gratton, E.; Prendergast, F. G. Resolvability of Fluorescence Lifetime Distributions Using Phase Fluorometry. *Biophys. J.* **1987**, *51*, 587-596.

(46) Lakowicz, J. R.; Cherek, H.; Gryczynski, I.; Joshi, N.; Johnson, M. L. Analysis of Fluorescence Decay Kinetics Measured in the Frequency Domain Using Distributions of Decay Times. *Biophys. Chem.* **1987**, *28*, 35-50.

(47) Gakamsky, D. M.; Goldin, A. a.; Petrov, E. P.; Rubinov, A. N. Fluorescence Decay Time Distribution for Polar Dye Solutions with Time-Dependent Fluorescent Shift. *Biophys. Chem.* **1992**, *44*, 47-60.

(48) Epstein, C. L.; Schotland, J. The Bad Truth About Laplace's Transform. *SIAM Rev.* **2008**, *50*, 504-520.

(49) Fogarty, A. C.; Jones, A. C.; Camp, P. J. Extraction of Lifetime Distributions from Fluorescence Decays with Application to DNA-Base Analogues. *Phys. Chem. Chem. Phys.* **2011**, *13*, 3819-3830.

(50) Wierzbinski, E.; de Leon, A.; Yin, X.; Balaeff, A.; Davis, K. L.; Reppireddy, S.; Venkatramani, R.; Keinan, S.; Ly, D. H.; Madrid, M.; Beratan, D. N.; Achim, C.; Waldeck, D. H. Effect of Backbone Flexibility on Charge Transfer Rates in Peptide Nucleic Acid Duplexes. *J. Am. Chem. Soc.* **2012**, *134*, 9335-9342.

(51) Venkatramani, R.; Davis, K. L.; Wierzbinski, E.; Bezer, S.; Balaeff, A.; Keinan, S.; Paul, A.; Kocsis, L.; Beratan, D. N.; Achim, C.; Waldeck, D. H. Evidence for a near-Resonant Charge Transfer Mechanism for Double-Stranded Peptide Nucleic Acid. *J. Am. Chem. Soc.* **2011**, *133*, 62-72.

(52) He, W.; Hatcher, E.; Balaeff, A.; Beratan, D. N.; Gil, R. R.; Madrid, M.; Achim, C. Solution Structure of a Peptide Nucleic Acid Duplex from Nmr Data: Features and Limitations. *J. Am. Chem. Soc.* **2008**, *130*, 13264-13273.

(53) Hornak, V.; Abel, R.; Okur, A.; Strockbine, B.; Roitberg, A.; Simmerling, C. Comparison of Multiple Amber Force Fields and Development of Improved Protein Backbone Parameters. *Proteins* **2006**, *65*, 712-725.

(54) Moret, M.-E.; Tavernelli, I.; Rothlisberger, U. Combined Qm/Mm and Classical Molecular Dynamics Study of [Ru(Bpy)3]2+ in Water. *J. Phys. Chem. B* **2009**, *113*, 7737-7744.

(55) Case, D. A.; Darden, T. A.; Cheatham, T. E. I.; Simmerling, C. L.; Wang, J.; Duke, R. E.; Luo, R.; Walker, R. C.; Zhang, W.; Merz, K. M.; Roberts, B.; Hayik, S.; Roitberg, A.; Seabra, G.; Swails, J.; Goetz, A. W.; Kolossváry, I.; Wong, K. F.; Paesani, F.; Vanicek, J.; Wolf, R. M.; Liu, J.; Wu, X.; Brozell, S. R.; Steinbrecher, T.; Gohlke, H.; Cai, Q.; Ye, X.; Hsieh, M.-J.; Cui,

G.; Roe, D. R.; Mathews, D. H.; Seetin, M. G.; Salomon-Ferrer, R.; Sagui, C.; Babin, V.; Luchko, T.; Gusarov, S.; Kovalenko, A.; Kollman, P. A.; University of California: San Francisco, 2012.

(56) Mergny, J. L.; Lacroix, L. Analysis of Thermal Melting Curves. *Oligonucleotides* **2003**, *13*, 515-537.

(57) Rehm, D.; Weller, A. Kinetics of Fluorescence Quenching by Electron and H-Atom Transfer. *Isr. J. Chem.* **1970**, *8*, 259-271.

(58) Tachiya, M. Energetics of Electron Transfer Reactions in Polar Solvents. *Chem. Phys. Lett.* **1994**, *230*, 491-494.

(59) Gray, H. B.; Winkler, J. R. Electron Transfer in Proteins. *Annu. Rev. Biochem.* **1996**, *65*, 537-561.

(60) Straume, M.; Frasier-Cadoret, S. G.; Johnson, M. L. Least-Squares Analysis of Fluorescence Data. *Top. Fluoresc. Spectrosc.* **1991**, *2*, 177-240.

(61) The upper limit (which is larger than 1010) of the equilibrium constant was studied by more accurate mechods such as ITC and UV titrations and it will be published in another paper. This communication focuses on the charge transfer thus only the low limit (which obtained by fitting the photoluminescence data to the bimolecular equilibrium model) is needed.

(62) Monzon, L. M. A.; Burke, F.; Coey, J. M. D. Optical, Magnetic, Electrochemical, and Electrical Properties of 8-Hydroxyquinoline-Based Complexes with Al 3+ , Cr 3+ , Mn 2+ , Co 2+ , Ni 2+ , Cu 2+ , and Zn 2+. *J. Phys. Chem. C* **2011**, *115*, 9182-9192.

(63) Kalyanasundaram, K. Photophysics, Photochemistry and Solar Energy Conversion with Tris(Bipyridyl)Ruthenium(Ii) and Its Analogues. *Coord. Chem. Rev.* **1982**, *46*, 159-244.

(64) Although the luminescence decay of the Ru complex in P-AG/Cu can be fit with a single exponential decay, the goodness of the fit can be increased by using a single modal distribution. The origin of the distribution is discussed later.

(65) Paul, A.; Watson, R. M.; Wierzbinski, E.; Davis, K. L.; Sha, A.; Achim, C.; Waldeck, D. H. Distance Dependence of the Charge Transfer Rate for Peptide Nucleic Acid Monolayers. *J. Phys. Chem. B* **2010**, *114*, 14140-14148.

(66) Daublain, P.; Thazhathveetil, A. K.; Wang, Q.; Trifonov, A.; Fiebig, T.; Lewis, F. D. Dynamics of Photochemical Electron Injection and Efficiency of Electron Transport in DNA. *J. Am. Chem. Soc.* **2009**, *131*, 16790-16797.

(67) Daublain, P.; Thazhathveetil, A. K.; Shafirovich, V.; Wang, Q.; Trifonov, A.; Fiebig, T.; Lewis, F. D. Dynamics and Efficiency of Electron Injection and Transport in DNA Using Pyrenecarboxamide as an Electron Donor and 5-Bromouracil as an Electron Acceptor. *J. Phys. Chem. B* **2010**, *114*, 14265-14272.

(68) Zimmt, M. B.; Waldeck, D. H. Exposing Solvent's Roles in Electron Transfer Reactions: Tunneling Pathway and Solvation. *J. Phys. Chem. A* **2003**, *107*, 3580-3597.

(69) Tachiya, M. Generalization of the Marcus Equation for the Electron-Transfer Rate. *J. Phys. Chem.* **1993**, *97*, 5911-5916.

(70) Shafirovich, V.; Dourandin, A.; Huang, W.; Luneva, N. P.; Geacintov, Q. N. E. Electron Transfer at a Distance Induced by Site-Selective Photoionization of 2-Aminopurine in Oligonucleotides and Investigated by Transient Absorption Techniques. *Phys. Chem. Chem. Phys.* **2000**, *2*, 4399-4408.

(71) Wagenknecht, H.-A. Electron Transfer Processes in DNA: Mechanisms, Biological Relevance and Applications in DNA Analytics. *Nat. Prod. Rep.* **2006**, *23*, 973-1006.

(72) Lewis, F. D.; Liu, X.; Liu, J.; Miller, S. E.; Hayes, R. T.; Wasielewski, M. R. Direct Measurement of Hole Transport Dynamics in DNA. *Nature* **2000**, *406*, 51-53.

(73) Kawai, K.; Takada, T.; Tojo, S.; Majima, T. Kinetics of Weak Distance-Dependent Hole Transfer in DNA by Adenine-Hopping Mechanism. *J. Am. Chem. Soc.* **2003**, *125*, 6842-6843.

(74) Lewis, F. D.; Wu, Y.; Zhang, L.; Zuo, X.; Hayes, R. T.; Wasielewski, M. R. DNA-Mediated Exciton Coupling and Electron Transfer between Donor and Acceptor Stilbenes Separated by a Variable Number of Base Pairs. *J. Am. Chem. Soc.* **2004**, *126*, 8206-8215.

(75) Behrens, C.; Burgdorf, L. T.; Schwögler, A.; Carell, T. Weak Distance Dependence of Excess Electron Transfer in DNA. *Angew. Chem., Int. Ed.* **2002**, *41*, 1763-1766.

(76) Elias, B.; Shao, F.; Barton, J. K. Charge Migration Along the DNA Duplex: Hole Versus Electron Transport. *J. Am. Chem. Soc.* **2008**, *130*, 1152-1153.

(77) Park, M. J.; Fujitsuka, M.; Kawai, K.; Majima, T. Direct Measurement of the Dynamics of Excess Electron Transfer through Consecutive Thymine Sequence in DNA. *J. Am. Chem. Soc.* **2011**, *133*, 15320-15323.

(78) Breeger, S.; Hennecke, U.; Carell, T. Excess Electron-Transfer-Based Repair of a Cis-Syn Thymine Dimer in DNA Is Not Sequence Dependent. *J. Am. Chem. Soc.* **2004**, *126*, 1302-1303.